J Solid State Eletrochem (2004) 8: 296–307
DOI 10.1007/s10008-003-0453-1

ORIGINAL PAPER

Su-Il Pyun · Jin-Ju Park

Fractal analysis of pit morphology of Inconel alloy 600 in sulphate, nitrate and bicarbonate ion-containing sodium chloride solution at temperatures of 25–100 °C

Received: 9 April 2003 / Accepted: 2 September 2003 / Published online: 21 November 2003

Abstract Pit morphology of Inconel alloy 600 in sulphate (SO_4^{2-}), nitrate (NO_3^-) and bicarbonate (HCO_3^-) ion-containing 0.5 M sodium chloride (NaCl) solution was analysed in terms of fractal geometry as functions of solution temperature and anion concentration using the potentiostatic current transient technique, scanning electron microscopy, image analysis and ac-impedance spectroscopy. Potentiostatic current transients revealed that the pitting corrosion is facilitated by the increase in solution temperature, irrespective of anion additives, and that it is hindered by the increase in NO_3^- and HCO_3^- ion concentration, regardless of solution temperature. Above 60 °C, it was also found that the addition of SO_4^{2-} ions impedes pit initiation, but enhances pit growth. The value of fractal dimension D_f of the pits increased with increasing solution temperature and with decreasing NO_3^- and HCO_3^- ion concentration. Moreover, the value of D_f increased above 60 °C with increasing SO_4^{2-} ion concentration. This is caused by the increase in the ratio of pit perimeter to pit area, implying the formation of pits with micro-branched shape due to the acceleration of the local attack in the pits. From the decrease of the depression parameter with increasing solution temperature, it is inferred that the roughness of the pits increased with increasing solution temperature. In addition, the depression parameter was found to increase with increasing NO_3^- and HCO_3^- ion concentration. But, above 60 °C, in the case of SO_4^{2-} ion addition, the depression parameter decreased with increasing SO_4^{2-} ion concentration. From the experimental findings, the three-dimensional pit morphology is discussed in terms of the values of D_f of the pits and the depression parameter, with respect to anion concentration and solution temperature.

Keywords Alloy 600 · Pit morphology · Solution temperature · Anion concentration · Fractal dimension · Depression parameter

S.-I. Pyun (✉) · J.-J. Park
Department of Materials Science and Engineering,
Korea Advanced Institute of Science and Technology,
373-1 Guseong-dong, Yuseong-gu,
Daejeon 305-701,
Republic of Korea
E-mail: sipyun@webmail.kaist.ac.kr
Tel.: +82 42-869-3319
Fax: +82 42-869-3310

Introduction

Inconel alloy 600 is a Ni-based alloy widely used as a steam generator tubing material in nuclear power plants. In this application, tube failures caused by pitting corrosion have been reported [1, 2, 3]. Thus, the study of pitting corrosion of alloy 600 is of great interest in both the industrial application and theoretical viewpoint.

The effects of solution temperature and anion additives on pitting corrosion have been studied extensively in view of changes in pitting potential and current density [4, 5]. Although such a number of studies have been made on pitting corrosion, little is known about the evolution of pit morphology. Since the shape of corrosion pits represents a time-averaged record of the anodic process which controls the corrosion rate [6, 7], the change in the morphology of the pits with different environmental conditions has been studied over time [8, 9].

In previous works [10, 11, 12], the effects of the addition of bicarbonate (HCO_3^-), nitrate (NO_3^-) and sulphate (SO_4^{2-}) ions on the morphological change of the pits formed on 316L stainless steel and pure aluminium were qualitatively investigated by observing the cross section of the pits. More recently, the morphological change of the pits formed on alloy 600 was examined quantitatively [13] as a function of solution temperature in terms of fractal geometry, which has been used to characterise such disorderly structures as fracture surface [14] and pit morphology [15, 16]. However, our previous works were related only to either the effect of anion additives or solution temperature. Thus, the effects of both the anion additives and solution

temperature on the morphological change of the pits in terms of fractal geometry are in question.

The objective of this work is to elucidate quantitatively the effect of such anion additives as SO_4^{2-}, NO_3^- and HCO_3^- ions on the morphological change in the pits formed on alloy 600 as functions of solution temperature and anion concentration by using fractal geometry. For this purpose, image analysis was employed to determine the fractal dimension of the two-dimensional pit morphology on the electrode surface. In addition, ac impedance measurements were carried out to measure the depression parameter that represents the roughness of the pits, i.e. three-dimensional pit morphology. The changes in the morphology of the pits are discussed in terms of the values of the fractal dimension and the depression parameter with respect to solution temperature and anion concentration.

Experimental

The specimen used in the present work was Inconel alloy 600 with the following composition (wt%): 15.4% Cr, 8.0% Fe, 0.3% Mn, 0.1% Si, 0.01% C and balance Ni. The specimen was set in a block of polyimid. The upper surface of the block was ground with emery paper, successively up to 2000 grit. The electrolytes used in this work were aqueous 0.5 M sodium chloride (NaCl) solutions containing sodium sulphate (Na_2SO_4), sodium nitrate ($NaNO_3$) and sodium bicarbonate ($NaHCO_3$) at concentrations of 0, 0.01, 0.03 and 0.05 M at temperatures of 25, 60 and 100 °C.

A three-electrode electrochemical cell was employed for electrochemical experiments. All electrochemical measurements at elevated solution temperatures were carried out using autoclave. A platinum wire was used as counter electrode and potentials were measured and controlled with an external silver/silver chloride (Ag/AgCl) reference electrode prepared by filling the entire compartment with 0.1 M KCl solution. The external reference electrode consisted of an Ag/AgCl electrode housed in a stainless steel compartment that was maintained at ambient temperature. The reference electrode compartment was connected to the high temperature autoclave by a high-pressure fitting. Working and counter electrodes were introduced into the autoclave through a high-pressure fitting.

To characterise the passivity of the oxide film and the pitting process of the electrode, the current density was recorded potentiostatically with time using a potentiostat/galvanostat (EG& G Model 263A) at an applied anodic potential of 1 $V_{Ag/AgCl}$. The specimen had an exposed area of 0.126 cm^2.

The morphology of corrosion pits formed on the specimen was examined as functions of solution temperature and anion concentration by using scanning electron microscopy (SEM). For the SEM observation, corrosion pits were made on the specimens by applying constant anodic potential of 1 $V_{Ag/AgCl}$ at various temperatures and anion concentrations. The pitted specimen was rinsed with distilled water and then cleaned with acetone immediately before SEM observation. After that, the observed pit morphology was digitised and pit perimeter and pit area were calculated from the digitised image by using a computer program, which was designed to detect up to 0.01 μm. The software was developed by Shin and Go [17] in our laboratory. Finally, the values of fractal dimension D_f for the various pits were determined by using the perimeter-area method [14, 18]. According to this method, the value of D_f of the pits is equivalent to just twice the value of the slope in the plot of pit perimeter vs. pit area on a logarithmic scale.

AC impedance measurements were conducted with a Solartron 1255 frequency response analyser connected to a Solartron 1287 electrochemical interface. In order to determine the depression parameter, first the pitted specimens were prepared electrochemically at 1 $V_{Ag/AgCl}$ for 500 s in aqueous 0.5 M NaCl solutions containing various anion concentrations at various solution temperatures; thereafter impedance spectra were recorded under open circuit conditions at room temperature in 0.5 M Na_2SO_4 solution. The depression parameter was determined using a complex nonlinear squares fitting method [19]. Impedance spectra were recorded from 10^5 Hz down to 10^{-1} Hz using 5 mV amplitude perturbations.

Results and discussion

Effects of solution temperature and anion concentration on the pitting corrosion of alloy 600

Figures 1a–c represent potentiostatic current transients obtained from alloy 600 subjected to a constant anodic potential of 1 $V_{Ag/AgCl}$ for 500 s in aqueous 0.5 M NaCl solution containing various SO_4^{2-}, NO_3^- and HCO_3^- ion concentrations, at 25 °C. The current transients were divided into two stages, i.e. the first pit initiation and growth stage and the second steady-state stage. In the first stage, it was found that the current density increased abruptly. This is caused by film breakdown due to the initiation and growth of the pits.

In the presence of anion additives in NaCl solution, after pit initiation, pitting corrosion product such as salt layer would be precipitated inside the pits. Then, a precipitated salt layer blocks up the pits and hence hinders the current flow through the pits. Therefore, a steady-state was attained between the metal dissolution and oxide film formation, including the barrier by precipitated salt layer in the second stage of the current transients. In other words, in the second stage, the increment in current density caused by the metal dissolution just equals the sum of the decrement in current density due to oxide film formation and the decrement of current density due to the barrier by precipitated salt layer, leading to nearly constant current density.

It can be seen from Fig. 1 that the value of slope of the first stage of the current transients decreased with increasing anion concentration. From this, as anion concentration increased in chloride solution, it can be said that the rate of growth of the pits decreased for all kinds of anion additives. In addition, it was also observed that steady-state current density decreased with increasing anion concentration. This implies that the pitting corrosion was suppressed by the addition of such anions as SO_4^{2-}, NO_3^- and HCO_3^- ions because of the competitive adsorption with Cl^- ions [20, 21].

Figures 2 and 3 give potentiostatic current transients obtained from alloy 600 subjected to a constant anodic potential of 1 $V_{Ag/AgCl}$ for 500 s in aqueous 0.5 M NaCl solution containing various anion concentrations at 60 and 100 °C, respectively. The current transients were similar in shape to those current transients obtained at room temperature. It was found that the value of steady-state current density in the second stage of the current transients increased with increasing solution temperature for all kinds of solutions. This stems from the

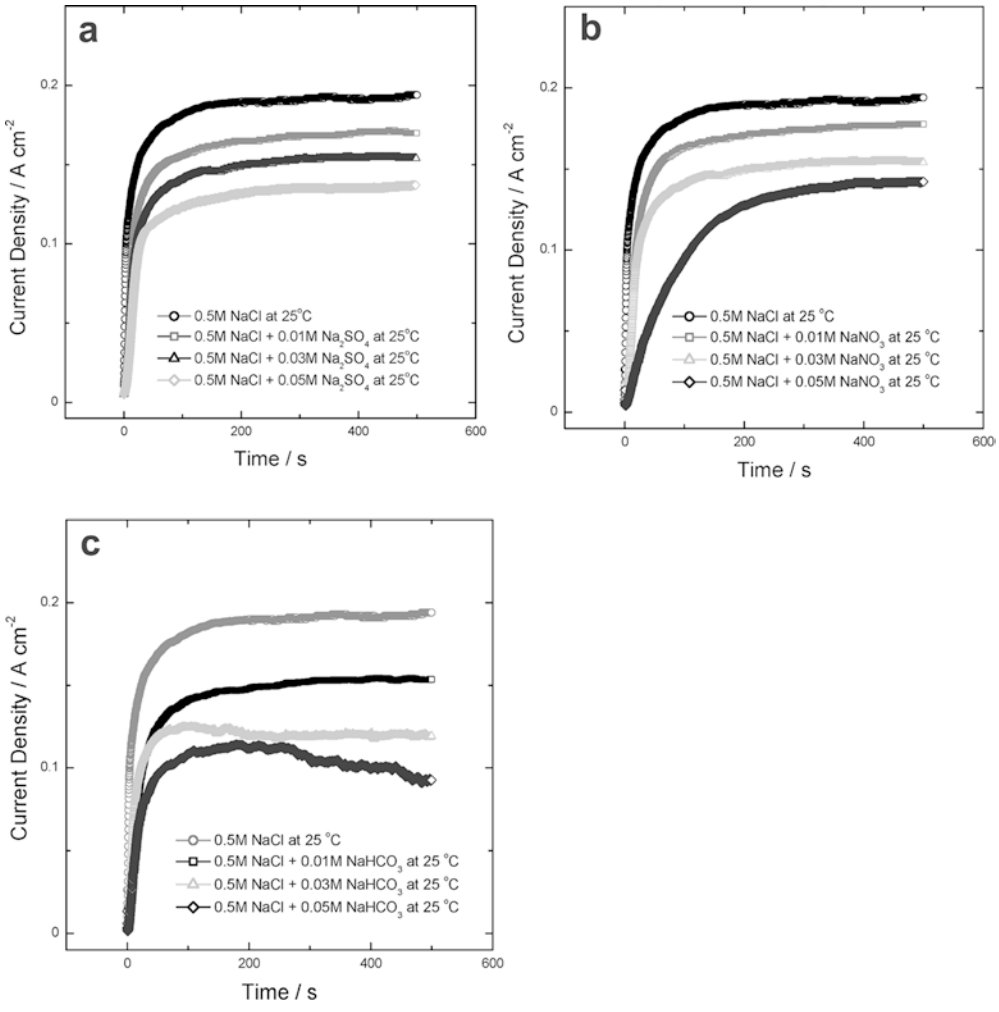

Fig. 1a–c Potentiostatic current transients of alloy 600 subjected to a constant anodic potential of 1 $V_{Ag/AgCl}$ for 500 s in aqueous 0.5 M NaCl solutions containing various concentrations of **a** Na_2SO_4, **b** $NaNO_3$ and **c** $NaHCO_3$ at 25 °C

acceleration of the growth of stable pits due to the decrease in the degree of passivity of oxide film formed on the specimen with increasing solution temperature [13].

In Fig. 3, it was observed that severe fluctuation of current density appeared in the second stage of the current transients. The occurrence of the current density fluctuation is due to two competing processes of the breakdown of passive film due to the decrease in the oxide film passivity and repassivation of the exposed metal surface due to the competitive adsorption of anion additives with Cl^- ions, i.e. current density increases by the formation of pit embryo, but it decreases by repassivation [22].

In Figs. 2 and 3, it should be noted that in the case of addition of SO_4^{2-} ions to NaCl solution, the steady-state current density increased with increasing SO_4^{2-} ion concentration, but in the case of addition of NO_3^- and HCO_3^- ions, steady-state current density decreased with increasing NO_3^- and HCO_3^- ion concentration.

For a better understanding of the effects of anion additives and solution temperature on pitting corrosion, the total charge per unit area consumed during the pitting corrosion was calculated by integrating the current density in potentiostatic current transients obtained at various anion concentrations and solution temperatures as shown in Figs. 1, 2 and 3, with respect to time for 500 s. The resulting total charge per unit area is given in Fig. 4 as functions of anion concentration and solution temperature. The value of the total charge was found to increase with increasing solution temperature for all kinds of solutions. This is because of the acceleration of the pitting corrosion due to the decrease in oxide film passivity at elevated solution temperature.

At room temperature, the total charge decreased with increasing anion concentration regardless of the kind of anion additive. This implies that the addition of SO_4^{2-}, NO_3^- and HCO_3^- ions to NaCl solution impedes the pitting corrosion. This is traced back to the competitive adsorption of anion additives with Cl^- ions. Above 60 °C, in the case of addition of NO_3^- and HCO_3^- ions, the total charge decreased with increasing NO_3^- and HCO_3^- ion concentration, similar to the case at room temperature, indicating the inhibiting effect of NO_3^- and HCO_3^- ions on pitting corrosion.

However, in the case of addition of SO_4^{2-} ions, it should be noted that SO_4^{2-} ions have two competing effects on the pitting process with respect to solution temperature. Figure 5 shows potentiostatic current transients on a magnified time scale for alloy 600 subjected to a

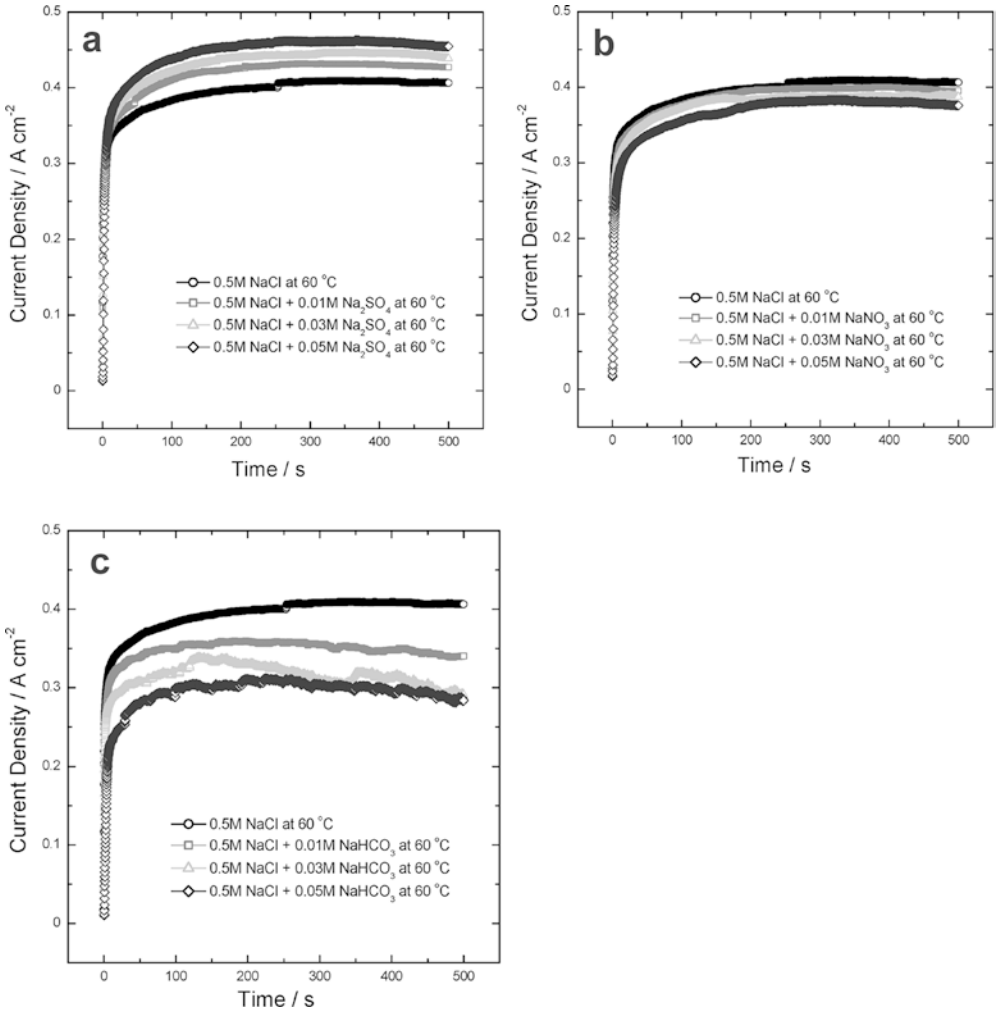

Fig. 2a–c Potentiostatic current transients of alloy 600 subjected to a constant anodic potential of 1 $V_{Ag/AgCl}$ for 500 s in aqueous 0.5 M NaCl solutions containing various concentrations of **a** Na_2SO_4, **b** $NaNO_3$ and **c** $NaHCO_3$ at 60 °C

constant anodic potential of 1 $V_{Ag/AgCl}$ in aqueous 0.5 M NaCl solutions containing various Na_2SO_4 concentrations at various solution temperatures. At 25 °C, it is easily seen from Fig. 5a that the current density decreased with increasing SO_4^{2-} ion concentration over the whole time. This means that the addition of SO_4^{2-} ions impedes the whole pitting processes, i.e. pit initiation and pit growth, at room temperature.

Above 60 °C, it was found that the current density decreased with increasing SO_4^{2-} ion concentration in the current density-ascending region, indicating the inhibiting effect of SO_4^{2-} ions on pit initiation. After that, the current density was found to increase with SO_4^{2-} ion concentration, implying the accelerating effect of SO_4^{2-} ions on pit growth after pit initiation.

In this work, these two competing effects of SO_4^{2-} ions on pit initiation and pit growth were experimentally verified by analysis of the SEM micrographs of pit morphology. Figure 6 gives typical SEM micrographs of pit morphology on the surface of alloy 600 subjected to a constant anodic potential of 1 $V_{Ag/AgCl}$ for 100 s in aqueous 0.5 M NaCl solutions containing various Na_2SO_4 concentrations at 100 °C. It can be seen from Fig. 6 that the number of pits per unit area, i.e. pit number density, decreased with increasing SO_4^{2-} ion concentration from 2812 pits/cm^2 at addition of 0.01 M SO_4^{2-} ions to 1875 pits/cm^2 at 0.05 M SO_4^{2-} ions. From this, it is realised that the addition of SO_4^{2-} ions impedes pit initiation.

In addition, the size of average pit area increased with SO_4^{2-} ion concentration from 3530 μm^2 at addition of 0.01 M SO_4^{2-} ions to 7084 μm^2 at 0.05 M SO_4^{2-} ions, which means that once corrosion pits are initiated above 60 °C, pit growth is accelerated by the addition of SO_4^{2-} ions. Consequently, it is inferred that the addition of SO_4^{2-} ions impedes the pit initiation, but it facilitates the pit growth after pit initiation.

It is necessary to discuss the tendency of total charge to increase as a result of an increase in SO_4^{2-} ion concentration above 60 °C. Considering that nickel (Ni) is the major alloying element of alloy 600, salt film formed on the specimen in the presence of SO_4^{2-} ions in NaCl solution is probably composed of nickel chloride ($NiCl_2$) and nickel sulphate ($NiSO_4$). From the facts that $NiSO_4$ is more soluble than $NiCl_2$ (as shown in Table 1 [23]) and SO_4^{2-} ions are more mobile than Cl^- ions (as shown in Table 2 [24]), it can be concluded that the inside of the pits was easily dissolved due to the preferential forma-

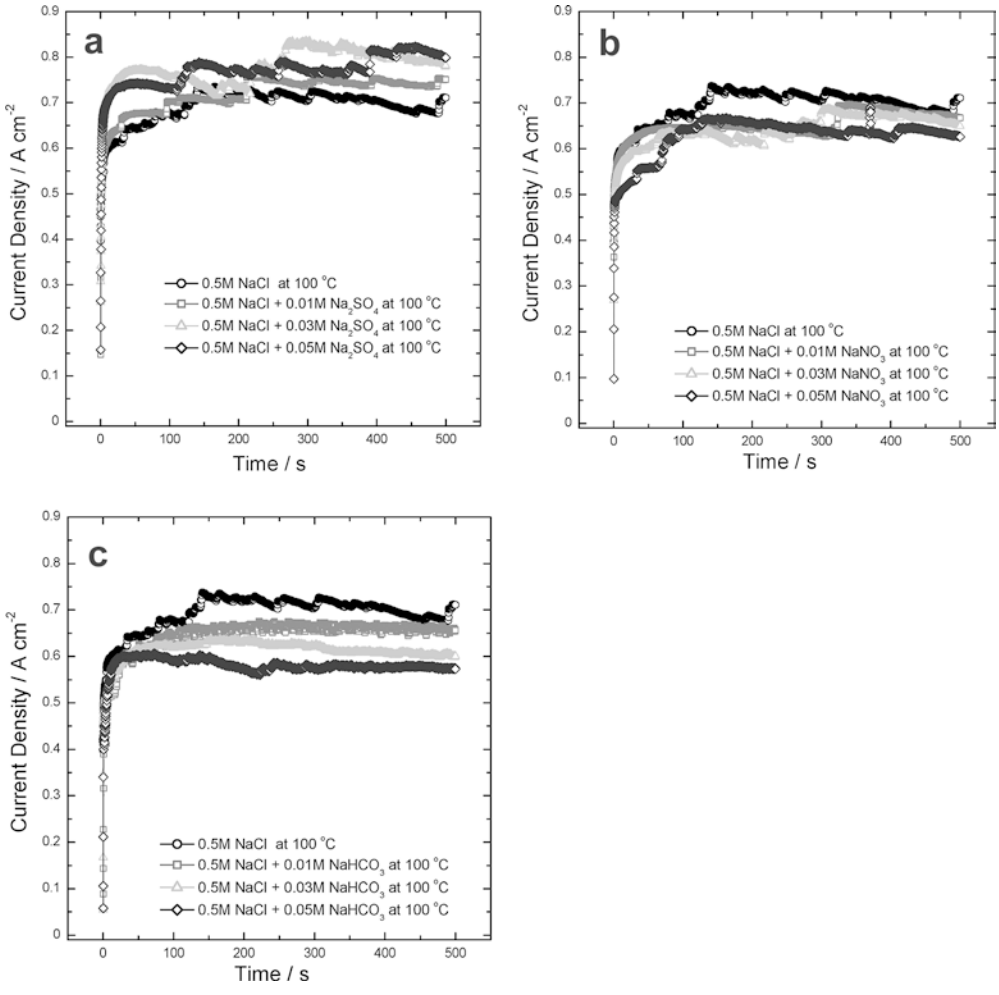

Fig. 3a–c Potentiostatic current transients of alloy 600 subjected to a constant anodic potential of 1 $V_{Ag/AgCl}$ for 500 s in aqueous 0.5 M NaCl solutions containing various concentrations of **a** Na_2SO_4, **b** $NaNO_3$ and **c** $NaHCO_3$ at 100 °C

tion of more soluble $NiSO_4$ salt film with increasing SO_4^{2-} ion concentration above 60 °C, resulting in the increase in the value of the total charge.

Characterisation of pit morphology by means of fractal dimension as functions of solution temperature and anion concentration

Figures 7a and b show typical SEM micrographs of pit morphology on the surface of alloy 600 subjected to a constant anodic potential of 1 $V_{Ag/AgCl}$ for 100 s in aqueous 0.5 M NaCl solution containing Na_2SO_4 concentrations of 0.01 and 0.05 M, respectively, at 25 °C. It was observed that pit morphology became more simplified at the pit rim with increasing SO_4^{2-} ion concentration. This means that the local attack at the pit rim was hindered by the addition of SO_4^{2-} ions to NaCl solution at room temperature due to the competitive adsorption of SO_4^{2-} ions with Cl^- ions.

Figures 8 and 9 give typical SEM micrographs of pit morphology on the surface of alloy 600 subjected to a constant anodic potential of 1 $V_{Ag/AgCl}$ for 100 s in aqueous 0.5 M NaCl solution containing various Na_2SO_4 concentrations at 60 and 100 °C, respectively. In contrast to the case at room temperature, it was noted that pit morphology became more complicated at the pit rim with increasing SO_4^{2-} ion concentration at elevated solution temperature, indicating the acceleration of the local attack at the pit rim. With higher solution temperature the effect would be much greater.

It should be stressed that from the viewpoint of fractal geometry, such irregular morphologies of the pits formed on the surface can be distinguishable from one another by means of the fractal dimension D_f, which is a non-integer value between 1 and 2 determined by the perimeter-area method. In other words, the degree of complexity of pit morphology can be quantitatively described by the value of D_f.

Figure 10 depicts typical logarithmic plots of perimeter vs. area for pit morphology on the surface of alloy 600 subjected to a constant anodic potential of 1 $V_{Ag/AgCl}$ for 100 s in aqueous 0.5 M NaCl solutions containing various concentrations of Na_2SO_4 at 25 °C. In this figure, linearity was observed between pit perimeter and pit area. It is generally known [14, 18] that twice the slope of the plot of pit perimeter against pit area on a logarithmic scale is the value of D_f of the pits. The values of D_f of the pits determined by the perimeter-area method are summarised in Fig. 11 as functions of

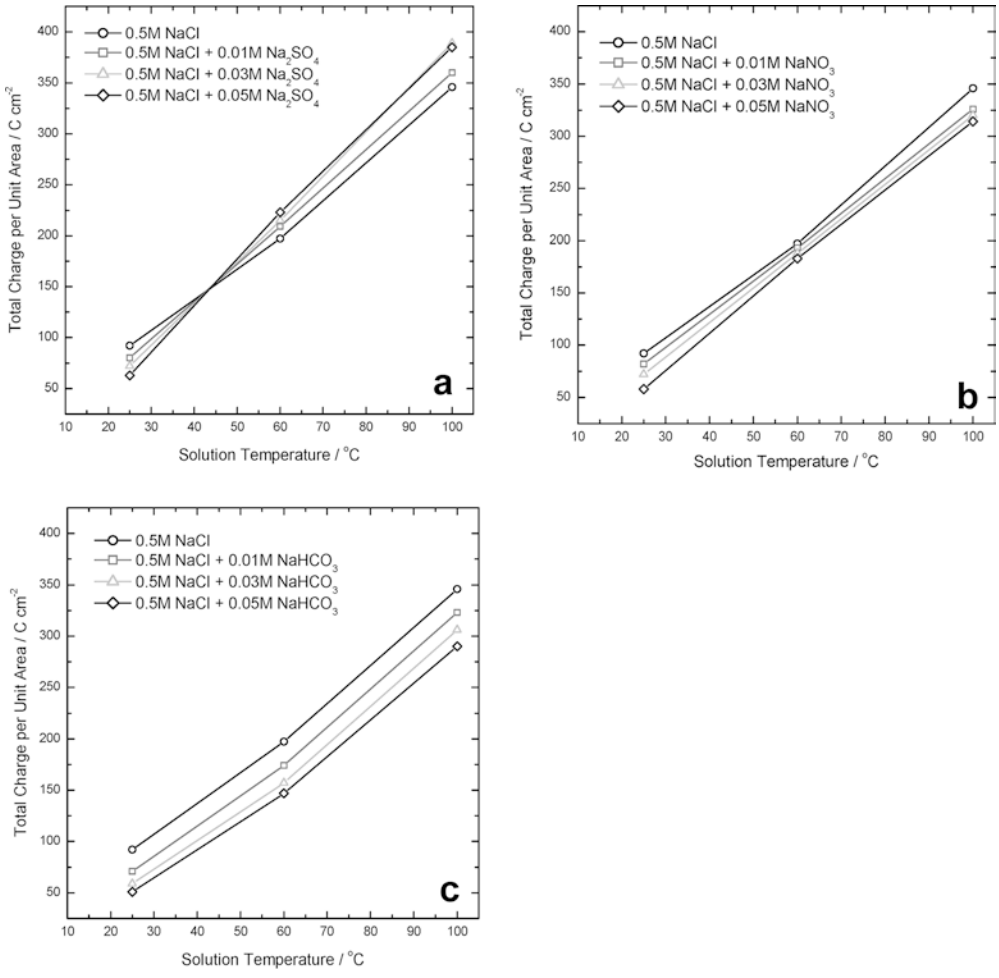

Fig. 4a–c Total charge per unit area consumed during pitting corrosion, calculated by integrating current density in potentiostatic current transients of Figs. 1, 2 and 3 with respect to time for 500 s in aqueous 0.5 M NaCl solutions containing various concentrations of **a** Na_2SO_4, **b** $NaNO_3$ and **c** $NaHCO_3$ at various solution temperatures

solution temperature and anion concentration. It is noted from Fig. 11 that increasing solution temperature raised the value of D_f of the pits, irrespective of the kind of anion additive. Higher D_f at higher solution temperature is due to the increase in the ratio of pit perimeter to pit area, indicating the formation of pits with micro-branched shape at the pit rim.

At 25 °C, the value of D_f of the pits decreased with increasing anion concentration. This means that the addition of SO_4^{2-}, NO_3^- and HCO_3^- ions to NaCl solution hinders the local attack by Cl^- ions at the pit rim as a result of the competitive adsorption with Cl^- ions. Accordingly, weakened local attack at the pit rim causes the reduction in pit perimeter and hence the value of D_f of the pits decreases with increasing anion concentration at room temperature.

Furthermore, above 60 °C, in the case of addition of NO_3^- and HCO_3^- ions, D_f of the pits decreased with increasing NO_3^- and HCO_3^- ion concentration, similar to the case at room temperature. By contrast, in the case of addition of SO_4^{2-} ions, D_f of the pits rose with increasing SO_4^{2-} ion concentration. From the result, it is readily inferred that the addition of NO_3^- and HCO_3^- ions to NaCl solution prevents the local attack, whereas the addition of SO_4^{2-} ions to NaCl solution enhances the local attack at elevated solution temperature.

Now, let us discuss the cut-off range in order to justify the value of D_f determined from pit morphology. Real bodies and surfaces can be modeled by fractals in a certain size range bordered by a cut-off range, i.e. inner cut-off and outer cut-off. In other words, in this work, the sizes of all kinds of pits should lie between the inner cut-off length and outer cut-off length in order to satisfy the fractal geometry. In the present work, it is very difficult to determine the cut-off ranges by means of the perimeter-area method. However, considering the length of yardstick and the diameter of the largest pit [13, 14, 25], inner cut-off length and outer cut-off length can be roughly estimated to be 0.01 μm and 128 μm, respectively. As a result, in the present work, since all of the pit sizes fall between the inner cut-off length and outer cut-off length, the value of D_f determined by the perimeter-area method satisfies the fractal characteristics.

Relationship between the depression parameter, the roughness of the pits and fractal dimension

Figure 12 envisages typical impedance spectra in Nyquist presentation obtained from alloy 600 at open circuit potential in aqueous 0.5 M Na_2SO_4 solution at room temperature after polarisation of 1 $V_{Ag/AgCl}$ for

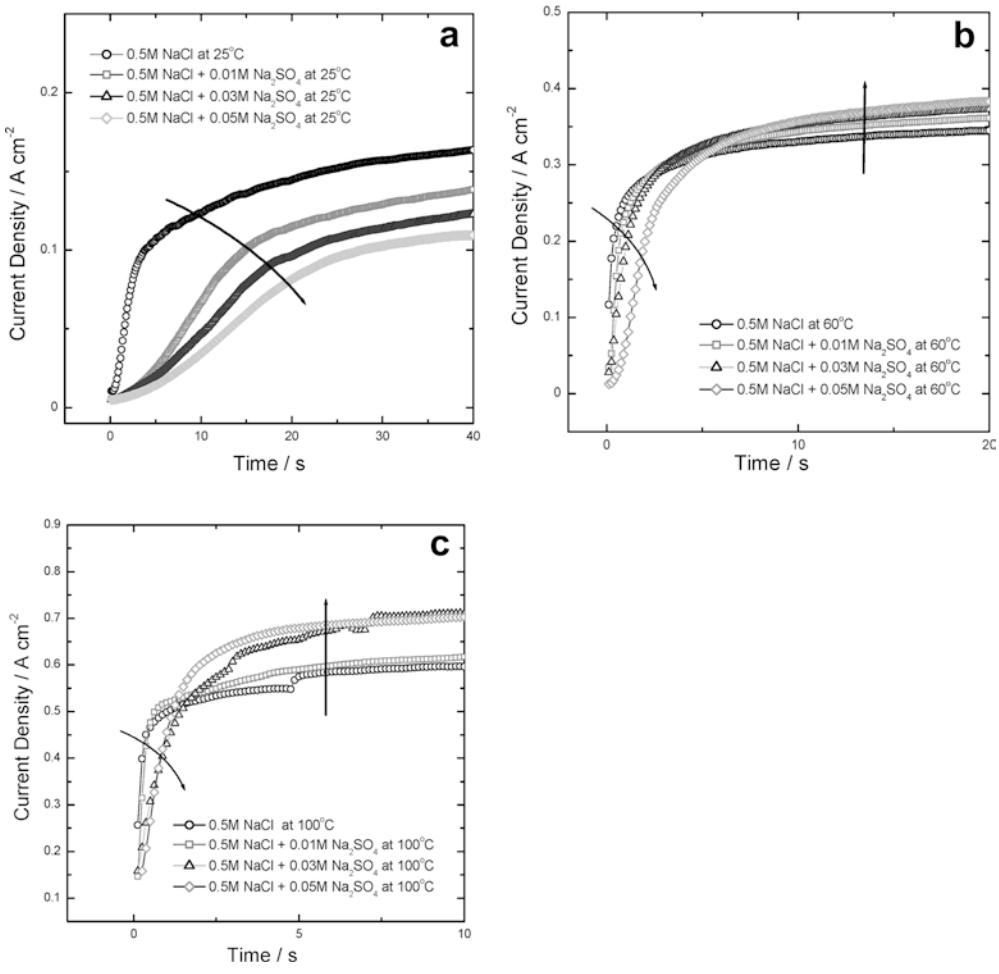

Fig. 5a–c Potentiostatic current transients on a magnified time scale for alloy 600 subjected to a constant anodic potential of 1 $V_{Ag/AgCl}$ in aqueous 0.5 M NaCl solutions containing various Na_2SO_4 concentrations at solution temperatures of **a** 25, **b** 60 and **c** 100 °C

100 s in 0.5 M NaCl solutions containing various concentrations of Na_2SO_4 at 60 °C. It is noted that the Nyquist plots were found to be depressed from a perfect semicircular form with increasing anion concentration. The depression of the impedance spectra from a perfect semicircle is ascribed to the enhancement of surface roughening effect of the specimen. This can be validated by the decrease in the depression parameter.

The impedance of a real electrode is frequently represented by an equivalent circuit containing a constant phase element (CPE) showing power law frequency dependence as follows [26, 27]:

$$Z_{CPE} = \frac{1}{C}(j\omega)^{-p}$$

where Z_{CPE} is the impedance of the CPE, C is the capacitance, p is the depression parameter and ω is the angular frequency. Figure 13 demonstrates changes in the value of the depression parameter, determined from impedance spectra of alloy 600 by using a complex nonlinear squares fitting method [19], as functions of anion concentration and solution temperature. The value of the depression parameter decreased with increasing solution temperature for all kinds of solutions.

In recent years, many researchers have demonstrated that the deviation from a perfect semicircular form observed on a real electrode is intimately related to surface irregularity and/or surface inhomogeneity [28, 29, 30, 31, 32, 33]. For instance, for a perfectly smooth and homogeneous surface at all scales, the value of the depression parameter is unity. In contrast, if there are surface irregularities, i.e. surface roughness and/or surface inhomogeneity (i.e. porous structure of oxide film), the depression parameter is lower than unity. It was found from Fig. 13 that the values of the depression parameter for all kinds of solutions are lower than unity. Therefore, it can be deduced that a lowered value of the depression parameter is due to surface roughness and/or to the existence of porous structure of oxide film.

In this respect, we should discuss which factor (roughness of the pits or porosity of the oxide film) is predominantly responsible for the change in the depression parameter. As solution temperature and concentration of anion additives vary, it should be noted that such oxide film properties as porosity and composition could also change. This means that the change in surface inhomogeneity might influence the value of the depression parameter.

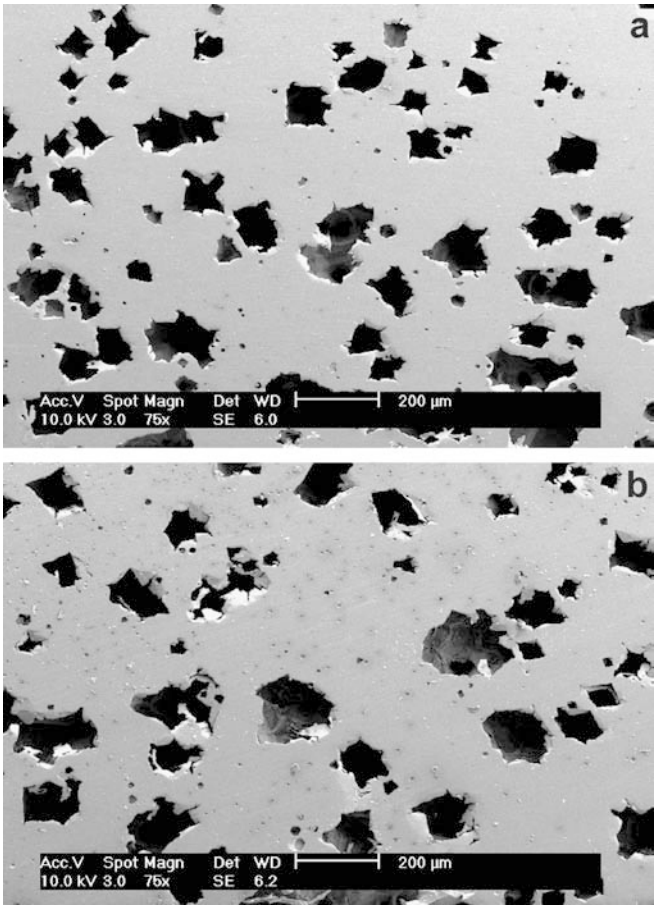

Fig. 6a,b Typical SEM micrographs of pit morphology on the surface of alloy 600 subjected to a constant anodic potential of 1 $V_{Ag/AgCl}$ for 100 s in aqueous 0.5 M NaCl solutions containing Na_2SO_4 concentrations of **a** 0.01 M and **b** 0.05 M at 100 °C

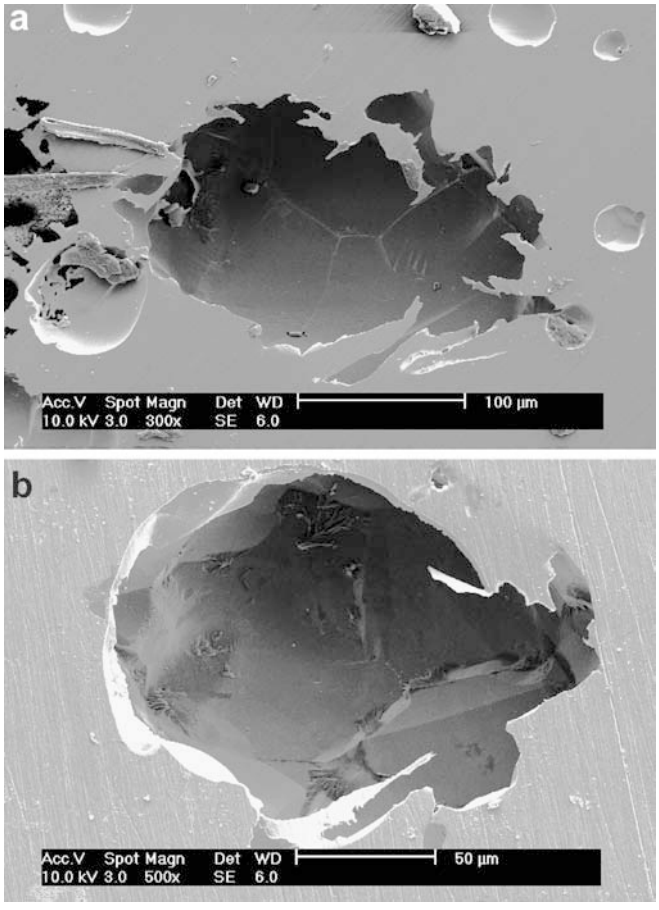

Fig. 7a,b SEM micrographs of pit morphology on the surface of alloy 600 subjected to a constant anodic potential of 1 $V_{Ag/AgCl}$ for 100 s in aqueous 0.5 M NaCl solutions containing Na_2SO_4 concentrations of **a** 0.01 M and **b** 0.05 M at 25 °C

Table 1 Solubilities of $NiCl_2$and $NiSO_4$ at various solution temperatures [23]

Salt	Solubility (g (100 mL)$^{-1}$)		
	25 °C	60 °C	100 °C
$NiCl_2$	39.6	44.8	46.7
$NiSO_4$	40.8	56.4	78.0

Table 2 Mobilities of Cl^- and SO_4^{2-} ions in water at various solution temperatures [24]

Ion	Mobility (cm^2 s^{-1} V^{-1})	
	25 °C	100 °C
Cl^-	7.9×10^{-4}	2.2×10^{-3}
SO_4^{2-}	8.3×10^{-4}	2.7×10^{-3}

Moreover, in this work, it is easily seen from Figs. 11 and 13 that the depression parameter is inversely proportional to the fractal dimension, irrespective of solution temperature and anion additives. Bearing in mind that the fractal dimension describes entirely the roughness of the pits, it is inferred that the depression parameter represents, crucially, the roughness of the pits. From the above arguments, it can be realised that surface inhomogeneity has little effect on the depression parameter. Consequently, it can be stated that the decrease in the depression parameter for the pitted specimen is mainly caused by the increase in the roughness of the pits with increasing solution temperature.

It was found that in the case of addition of NO_3^- and HCO_3^- ions, the depression parameter increased with increasing NO_3^- and HCO_3^- ion concentration, irrespective of solution temperature. This implies that the addition of NO_3^- and HCO_3^- ions to NaCl solution reduces the roughness of the pits. In the case of addition of SO_4^{2-} ions, at room temperature, the depression parameter increased with increasing SO_4^{2-} ion concentration, but the depression parameter decreased with SO_4^{2-} ion concentration above 60 °C. This implies that SO_4^{2-} ion addition makes the electrode surface more roughened due to the promotion of pit growth at elevated solution temperature.

At this point, it is necessary to clarify the relationship between the D_f and the depression parameter. In the present work, it should be emphasised that since the

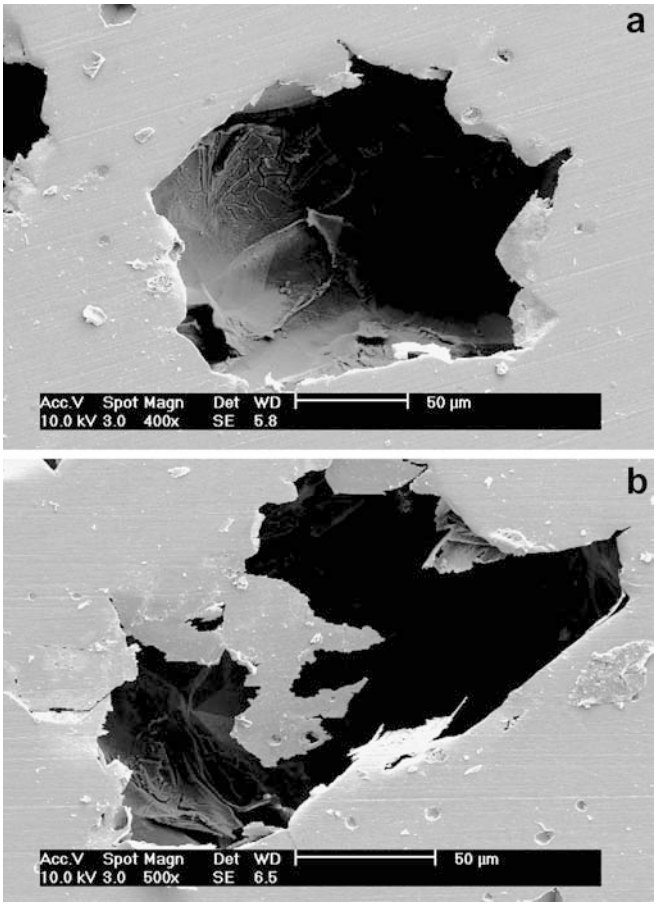

Fig. 8a,b SEM micrographs of pit morphology on the surface of alloy 600 subjected to a constant anodic potential of 1 $V_{Ag/AgCl}$ for 100 s in aqueous 0.5 M NaCl solutions containing Na_2SO_4 concentrations of **a** 0.01 M and **b** 0.05 M at 60 °C

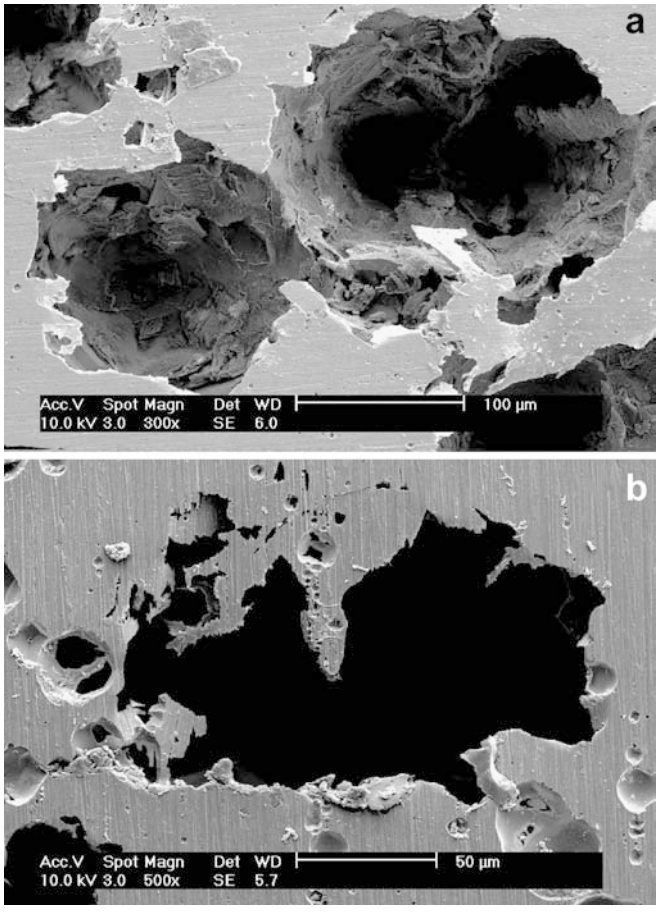

Fig. 9a,b SEM micrographs of pit morphology on the surface of alloy 600 subjected to a constant anodic potential of 1 $V_{Ag/AgCl}$ for 100 s in aqueous 0.5 M NaCl solutions containing Na_2SO_4 concentrations of **a** 0.01 M and **b** 0.05 M at 100 °C

value of D_f determined by the perimeter-area method represents the degree of complexity of the two-dimensional pit morphology on the surface as a number, it cannot give information about the morphology of the inside of the pits. On the other hand, the depression parameter depicts the roughness of the pits, i.e. the three-dimensional pit morphology.

It is generally agreed [30] that the value of D_f is inversely proportional to the value of the depression parameter. In the present work, from the experimental findings, it was noted that the depression parameter shows a reverse tendency compared with D_f for all kinds of solutions. From this, we can visualise the three-dimensional pit morphology, including the inside of the pits, in terms of the changes in the value of D_f. As a result, it is concluded that the inside of the pits shows the same tendency to change in the morphology as the two-dimensional pit morphology observed only on the electrode surface.

Above 100 °C, since it is very difficult to determine D_f by using the perimeter-area method, it is hard to quantitatively characterise the pit morphology by means of D_f. However, from the observation of more complicated morphology of the pits in Cl^- ion-containing solution above 100 °C in the previous work [13], it is expected that the D_f of the pitted surface increased in series with increasing solution temperature. Therefore, it can be

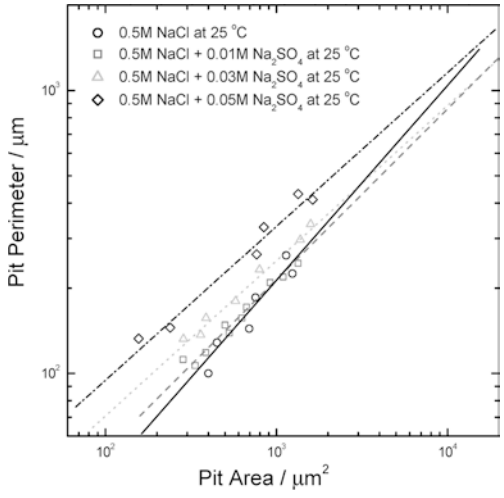

Fig. 10 Typical logarithmic plots of perimeter vs. area for the pit morphology on the surface of alloy 600 subjected to a constant anodic potential of 1 $V_{Ag/AgCl}$ for 100 s in aqueous 0.5 M NaCl solutions containing various concentrations of Na_2SO_4 at 25 °C

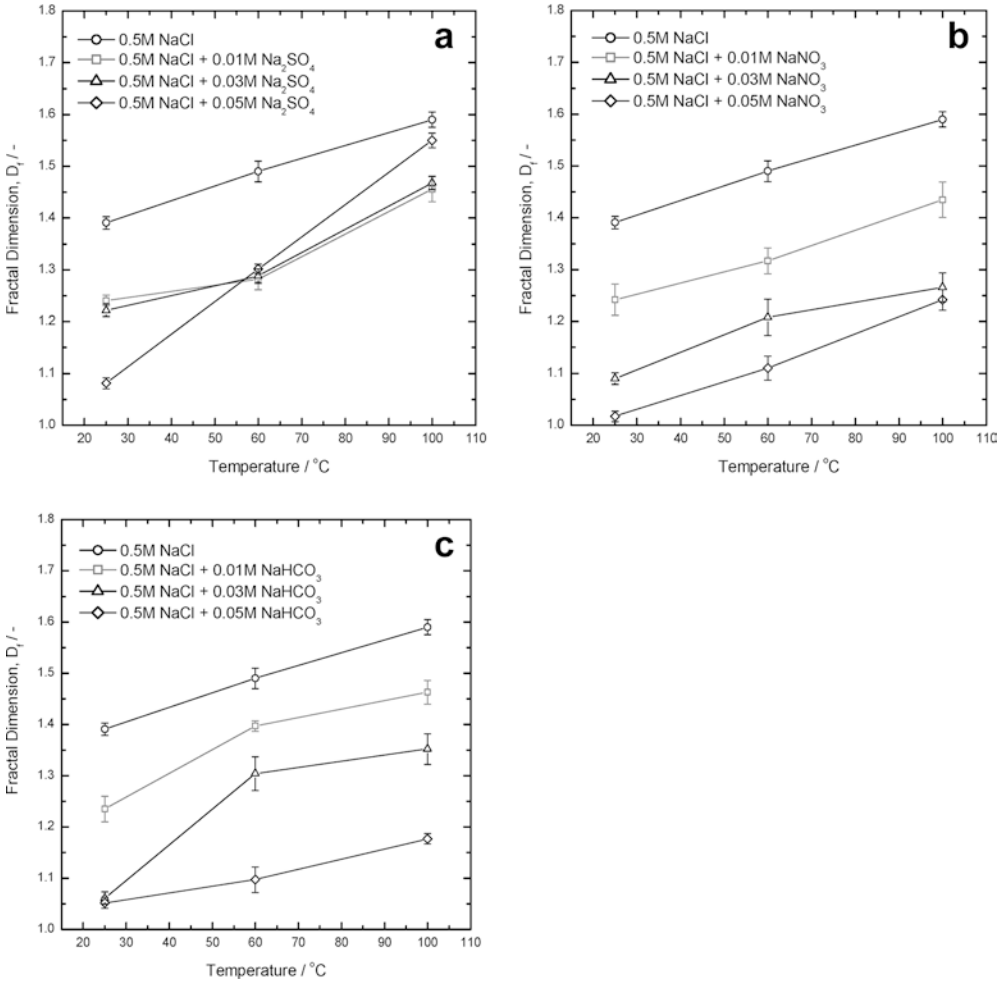

Fig. 11a–c Changes in the value of fractal dimension D_f determined by the perimeter-area method for the pit morphology on the surface of alloy 600 subjected to a constant anodic potential of 1 $V_{Ag/AgCl}$ for 100 s in aqueous 0.5 M NaCl solutions containing various concentrations of **a** Na_2SO_4, **b** $NaNO_3$ and **c** $NaHCO_3$ at various solution temperatures

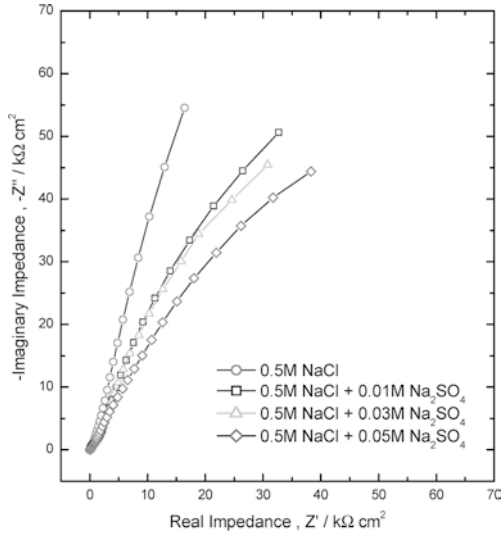

Fig. 12 Typical impedance spectra in Nyquist presentation obtained from alloy 600 at open circuit potential in aqueous 0.5 M Na_2SO_4 solutions at room temperature after polarisation of 1 $V_{Ag/AgCl}$ for 100 s in 0.5 M NaCl solutions containing various concentrations of Na_2SO_4 at 60 °C

stated that the temperature dependences of the D_f and the depression parameter shown in anion-containing chloride solution below 100 °C could also be applicable to the same solution at higher solution temperatures, ranging from 300 to 350 °C.

Conclusions

1. As solution temperature increased, the values of the total charge and fractal dimension increased and, at the same time, the value of the depression parameter decreased for all kinds of anion additives. This is ascribed to the increase in the roughness of the pits due to the acceleration of the pitting corrosion at elevated solution temperature.
2. In the case of addition of NO_3^- and HCO_3^- ions, the values of the total charge and fractal dimension decreased and, simultaneously, the value of the depression parameter increased with increasing NO_3^- and HCO_3^- ion concentration, irrespective of solution temperature. This implies that the pitting corrosion was suppressed by the addition of NO_3^- and HCO_3^- ions due to the competitive adsorption

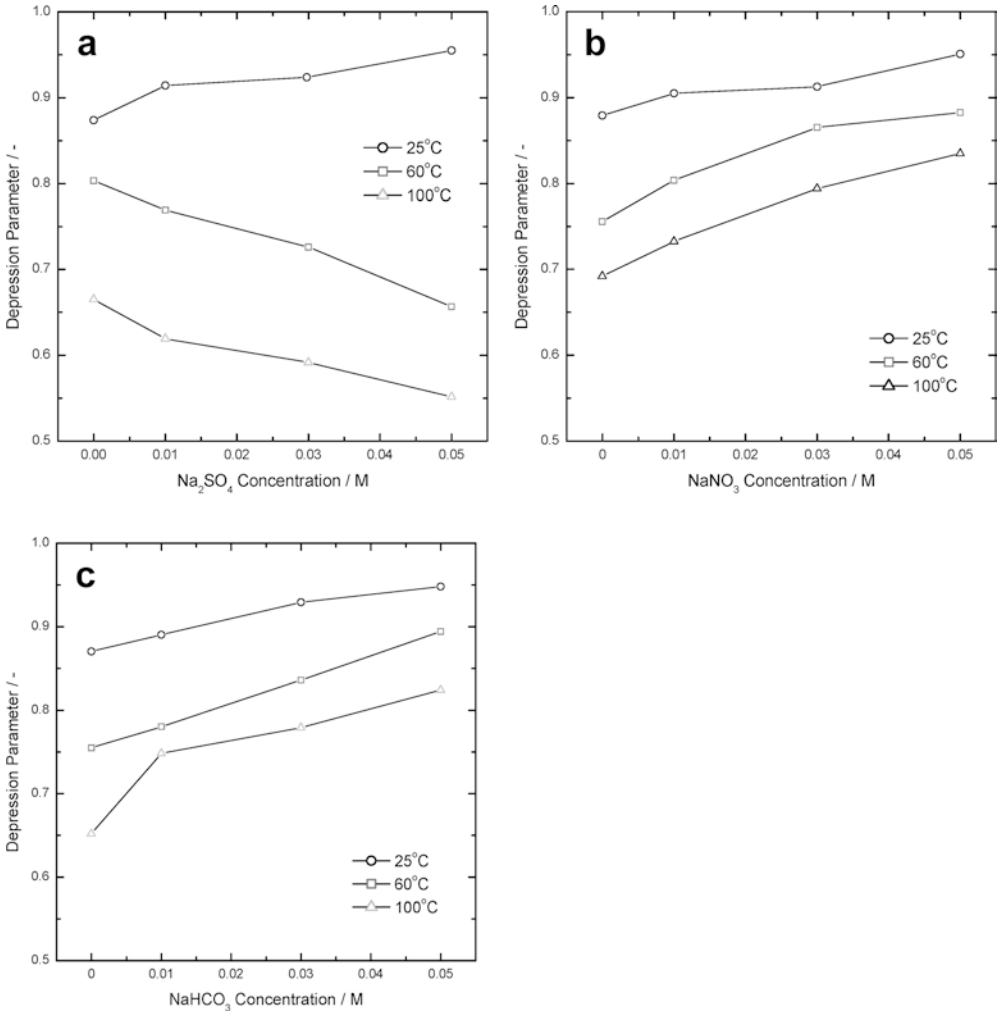

Fig. 13a–c Changes in the value of the depression parameter p determined from impedance spectra of alloy 600 obtained at open circuit potential in aqueous 0.5 M Na_2SO_4 solutions at room temperature after polarisation of 1 $V_{Ag/AgCl}$ for 100 s in 0.5 M NaCl solutions containing various concentrations of **a** Na_2SO_4, **b** $NaNO_3$ and **c** $NaHCO_3$ at various solution temperatures

with Cl^- ions. As a result, the local attack on the electrode surface was hindered and hence the roughness of the pits decreased with increasing NO_3^- and HCO_3^- ion concentration.

3. In the case of addition of SO_4^{2-} ions, above 60 °C, the addition of SO_4^{2-} ions impedes pit initiation, but it enhances pit growth after pit initiation. As a result of the enhancement of pit growth by SO_4^{2-} ions, the total charge, fractal dimension and the depression parameter showed a reverse tendency compared with addition of NO_3^- and HCO_3^- ions. Consequently, it is concluded that the addition of SO_4^{2-} ions to NaCl solution accelerates the local attack on the electrode at elevated solution temperature, leading to the increase in the roughness of the pits.
4. From the finding that the depression parameter is inversely proportional to the fractal dimension for all kinds of solutions, it is concluded that the three-dimensional pit morphology, including the inside of the pits, can be described by the change in the fractal dimension.

Acknowledgements One of the authors (JJP) would like to thank to Mr. J.-S. Oh at the CIERL, KAIST for his great help with electrochemical experiments. This work was partly supported by the Brain Korea 21 project.

References

1. Ho JT, Yu GP (1992) Corrosion 48:147
2. Choi D, Was GS (1992) Corrosion 48:292
3. Chang MY, Yu GP (1993) J Nuc Mat 202:145
4. Bohni H, Uhlig HH (1969) J Electrochem Soc 116:906
5. Curley-Fiorino ME, Schmid GM (1980) Corros Sci 20:313
6. Reiser DB, Alkire RC (1984) Corros Sci 24:579
7. Alkire RC, Wong KP (1988) Corros Sci 28:411
8. Was GS, Choi D (1992) Corrosion 48:103
9. Mankowski G, Duthil JP, Giusti A (1997) Corros Sci 39:27
10. Park JJ, Pyun SI, Lee WJ, Kim HP (1999) Corrosion 55:380
11. Pyun SI, Na KH, Lee WJ, Park JJ (2000) Corrosion 56:1015
12. Pyun SI, Na KH, Park JJ (2000) J Solid State Electrochem 5:473
13. Park JJ, Pyun SI (2003) Corros Sci 45:995
14. Mandelbrot BB, Passoja DE, Paullay AJ (1984) Nature 308:721
15. Costa JM, Sagues F, Vilarasa M (1991) Corros Sci 32:665
16. Proost J, Baklanov M, Verbeeck R, Maex K (1998) J Solid State Electrochem 2:150
17. Shin HC, Go JY (2001) private communication, KAIST, Daejeon, Republic of Korea
18. Feder J (1988) Fractals. Plenum, New York, p 200
19. Bae JS, Pyun SI (1994) J Mat Sci Lett 13:573

20. Kolics A, Polkinghorne JC, Wieckowski A (1998) Electrochim Acta 43:2605
21. Pyun SI, Moon SM (1999) J Solid State Electrochem 3:331
22. Kobayashi Y, Virtanen S, Bohni H (2000) J Electrochem Soc 147: 155
23. Linke WF (1958) Solubilities, inorganic and metal organic compounds: a compilation of solubility data from the periodical literature. Van Nostrand, Princeton, NJ, p 1208, 1219
24. David DL (1985) Handbook of aqueous electrolyte solutions. Wiley, New York, p 240
25. Normant F, De Walle AV (1996) Cartographica 33:1
26. Macdonald JR (1987) Impedance spectroscopy. Wiley, New York, p 17
27. Piela B, Worna PK (1995) J Electroanal Chem 388:69
28. Pajkossy T, Nyikos (1986) J Electrochem Soc 133:2061
29. Halsey TC (1987) Phys Rev A 35:3512
30. Rammelt U, Reinhard G (1987) Corros Sci 27:373
31. Hill RM, Dissado LA (1988) Solid State Ionics 26:295
32. Mulder WH, Sluyters JH (1988) Electrochim Acta 33:303
33. Pajkossy T (1994) J Electroanal Chem 364:111